NASA-CR-203706

Scattered light characteristics of the *Hubble Space Telescope* Faint Object Spectrograph

F. Bartko

Bartko Science & Technology, P. O. Box 608, Castle Rock, CO 80104

G. Burks

University of Colorado, CASA, C. B. 389, Boulder, CO, 80302

G. Kriss and A. Davidsen

John Hopkins University, Baltimore, MD, 21218

R. Cohen, V. Junkkarinen, R. Lyons

CASS, University of California San Diego, La Jolla, CA 90293

R. Harms

Applied Research Corporation, Landover, MD 20715

ABSTRACT

Observations of a standard star (BD+75D325) have been used to measure the Hubble Space Telescope (HST)/ Faint Object Spectrograph (FOS) scattering characteristics in the wavelength range 115 to 250 nm. Spectra of the standard star were obtained as the star was progressively offset from the optical line of sight axis of the telescope, both in the in-dispersion and cross-dispersion directions.

These data have been reduced and analyzed to determine the scattering function of the telescope-spectrograph combination. Two primary results have been obtained. (1) The resulting scattering function exhibits three characteristics: (a) The inner core ($\theta < 4''$) is dominated by the large Point Spread Function (PSF) of the HST; (b) the outer wings of the scattering function ($4'' < \theta < 32''$) show a θ^{-3} dependence consistent with predictions for the HST Airy disc; and (c) The wavelength dependence of this scattering function follows λ^{-1}, suggesting that the ultraviolet (UV) micro roughness contribution to the scatter is quite small, and hence the HST primary mirror is very smooth at ultraviolet wavelengths. (2) The FOS scattering contribution is limited only by grating scatter, and is consistent with pre-launch grating calibration measurements.

1. INTRODUCTION

The Faint Object Spectrograph (FOS)[6,7,8] on the Hubble Space Telescope (HST)[3] has been used to measure the scattering characteristics arising from their combined optical paths. The measurement is part of the Science Verification observations (SV 1319) performed during the early phases of HST operations.

A specific test was suggested by W. Fastie and devised by A. Davidsen for the *HST*-FOS. In this test, a bright star is measured on axis, and then incrementally offset in several steps. A spectrum of the star is recorded at each off axis position. We determined the scattering characteristics by observing a standard star (BD +75D325, spectral type = 05p, V = 9.54, B-V = 0.32), as suggested, at a series of predetermined offset positions, both in the in-dispersion and the orthogonal cross dispersion directions. The resulting spectra were processed with the STSDAS CALFOS routine at the Space Telescope Science Institute (STScI) and refined at UCSD. This report describes the details of the observations that were made, the reduction procedures that were applied to the data, and the results and conclusions that

0-8194-1181-7/93/$6.00

were derived from the analysis of the reduced data.

A "red leak" scattered light test has been considered and analyzed by Blair et al.[1] and Uomoto et al. [1] and reported elsewhere. Also, Caldwell [4,5] compared the FOS UV response with the GHRS UV response to a bright solar type star, and observed out of order scatter due to the FOS gratings, at a level which is consistent with the results reported here.

2. OBSERVATIONS

The observations for this science verification test were obtained on March 9th and 10th of 1991. All observations were obtained with the FOS Blue Digicon detector. Since the standard star BD+75D325 is too bright for a binary search acquisition with the camera mirror, a series of peak up acquisitions, were used to center the star in the FOS apertures, with the FOS configured to the G130H grating.

The FOS was then configured to the G160L low resolution mode, (R ≈ 200) grating, the 1.0 arc sec aperture, and the ACCUM data mode (XSTEPS = 4, OVERSCAN = 5, INTS = 1, SLICES = 1, PATTERNS = 1; and livetime parameters were varied to provide the desired integration times). With the standard star centered in the aperture, a 1 sec exposure was obtained for the on-axis reference spectrum. The HST was then commanded to offset the standard star from the telescope optical axis in various angular increments, in the in-dispersion direction, according to the offsets indicated in Table 1. As the telescope offsets the standard star from the telescope optical axis, the integration times and apertures are adjusted to maintain an adequate level of counts for good signal to noise ratio.

The same procedure was repeated for the cross-dispersion direction. The standard star was again acquired and centered in the aperture through a series of target acquisition peak ups, followed by the ACCUM data mode to obtain spectra of the standard star at the same set of offset positions.

The data log for this entire set of observations is shown in Table 2. The root name of the data files are identified for each set of measurements described. The Y0HW0101T - Y0HW0103T files are the target acquisition data. The Y0HW0104T - Y0HW010BT files are the spectra obtained for each desired off set position in the in-dispersion direction. The Y0HW020* series are the data files for the corresponding positions in the cross dispersion direction.

Table 1. Standard Star Observations

Aperture	Integration Time(sec)	Offset Angle(arc sec)
A1.0	5	1.0
A1.0	20	2.0
A1.0	100	4.0
A4.3	10	4.0
A4.3	60	8.0
A4.3	480	16.0
A4.3	960	32.0

Table 2. SV1319 Data Log

Faint Object Spectrograph (FOS) Observation Log

Entry	Root name	Date	DETEC	fgw	ap	YBASE	DISK	Target name
4062	Y0HW0101T	09/03/91	BLUE	H13	B-3	-677	6b	BD+75D325
4063	Y0HW0102T	09/03/91	BLUE	H13	B-2	-677	6b	BD+75D325
4064	Y0HW0103T	09/03/91	BLUE	H13	B-2	-677	6b	BD+75D325
4065	Y0HW0104T	09/03/91	BLUE	L15	B-3	-920	6b	BD+75D325
4066	Y0HW0105T	09/03/91	BLUE	L15	B-3	-920	6b	BD+75D325
4067	Y0HW0106T	09/03/91	BLUE	L15	B-3	-920	6b	BD+75D325
4068	Y0HW0107T	09/03/91	BLUE	L15	B-3	-920	6b	BD+75D325
4069	Y0HW0108T	09/03/91	BLUE	L15	A-1	-920	6b	BD+75D325
4070	Y0HW0109T	09/03/91	BLUE	L15	A-1	-920	6b	BD+75D325
4071	Y0HW010AT	09/03/91	BLUE	L15	A-1	-920	6b	BD+75D325
4072	Y0HW010BT	09/03/91	BLUE	L15	A-1	-920	6b	BD+75D325
4073	Y0HW0201T	09/03/91	BLUE	L15	B-3	-677	6b	BD+75D325
4074	Y0HW0202T	09/03/91	BLUE	H13	B-2	-677	6b	BD+75D325
4075	Y0HW0203T	09/03/91	BLUE	H13	B-2	-677	6b	BD+75D325
4076	Y0HW0204T	09/03/91	BLUE	H13	B-3	-920	6b	BD+75D325
4077	Y0HW0205T	09/03/91	BLUE	L15	B-3	-920	6b	BD+75D325
4078	Y0HW0206T	09/03/91	BLUE	L15	B-3	-920	6b	BD+75D325
4078	Y0HW0207T	09/03/91	BLUE	L15	B-3	-920	6b	BD+75D325
4079	Y0HW0208T	09/03/91	BLUE	L15	A-1	-920	6b	BD+75D325
4082	Y0HW0209T	09/03/91	BLUE	L15	A-1	-920	6b	BD+75D325
4082	Y0HW020AT	10/03/91	BLUE	L15	A-1	-920	6b	BD+75D325
4082	Y0HW020BT	10/03/91	BLUE	L15	A-1	-920	6b	BD+75D325

3. DATA REDUCTION AND ANALYSIS

All data were processed through selected portions of the data reduction package CALFOS at the Space Telescope Science Institute, and later refined at UCSD. Using FOS calibration data, CALFOS performs various operations on the raw data files, such as bad pixel removal, flat field corrections, dark count subtraction, wavelength calibration, and conversion of data files from counts versus pixels to fluxes versus wavelength, using inverse sensitivity calibration values. The IRAF data reduction system was then used to further reduce and analyze the data.

Using IRAF routines such as *splot*, the spectra were displayed and subsequently processed. The raw spectra that we obtained are collected and shown in Figure 1 for the in-dispersion measurements. The cross dispersion measurements are very similar, and hence not included here.

For each set, the series of offset spectra were first normalized by their integration times to convert the data to count rates, and then subsequently normalized by effective aperture area. Once the data were normalized, we then took the spectrum for each of the offset positions, and divided them by the on-axis reference spectrum. The divided spectra then gave residual spectral count rates at each off-set location.

The normalized spectral count rates exhibit a number of noteworthy features. First, there is a slight color dependence (especially for the larger offset positions θ>4") i.e. the residual count rates, at 120 nm, are approximately twice the value at 240 nm). Second, the geocoronal Lyman alpha emission appears in both first and second order, when the change over to the large aperture (4.3 arc sec) occurs at the offset pointing location of 4.0 arc secs.

To analyze the data further, we selected 4 spectral wavelength bins in each of the residual spectra shown. These regions are: (1) 95-110 nm (which should contain no light since the detector faceplate window (MgF_2) transmission cuts off at 115 nm), (2) 125 to 140 nm (excludes 1st order geocoronal Lyman Alpha), (3) 170-190 nm, and (4) 225-240 nm (excludes 2nd order geocoronal Lyman Alpha. We then ran the IRAF task *splot* to calculate the mean count rates in each of these wavelength bins at each offset location. These mean count rates were then collected and plotted using the IRAF task *graph*. The results are given in Figures 2 and 3, and show the mean residual count rates at each offset location, as a function of the offset location.

Figure 2 shows the mean residual count rate for spectral intervals (2), (3), and (4) defined above, versus offset position. The jagged feature shown at the 4.0 arc sec offset location is due to the changeover from the 1.0 arc sec aperture to the larger 4.3 arc sec aperture.

A similar procedure was followed for the cross-dispersion data. Figure 3 shows the cross-dispersion data compared with the in-dispersion data for the wavelength bins 170-190 nm and 95-110 nm. Note the offset between spectral bin (1) and spectral bin (3). Here, the ratio of the mean count rate in 170-190 nm to the mean count rate in 95-110 nm is approximately 350, a value which is consistent with independent, pre-flight measurement of the FOS grating at Johns Hopkins University.

The scattering function derived is essentially azimuthally symmetric except in the inner core. This is due to the fact that the pixel dimensions are different in the in-dispersion (40 μm wide, corresponding to 0.25 arc sec) and the cross dispersion direction (140 μm high corresponding to 1.4 arc sec). Hence, as the star image is offset in either direction, the diodes will be illuminated differently.

4. RESULTS AND DISCUSSION

Several properties of the scattering function derived in the previous section are noted here. First, the decrease in the scattering function in the inner core ($\theta < 4''$) is dominated by the HST point spread function (PSF), while the outer wings ($4'' < \theta < 32''$) are dominated by HST primary mirror scatter. According to Brown and Burrows[2], and Hasan [9], the far wings of this function are composed of a combination of Airy disk (θ^{-3}) and surface microroughness ($\theta^{-2.19}$) contributions. We have fit the wings of the scattering function seen in Figure 4, and have determined an angular dependence of θ^{-3}, consistent with the theoretical predictions for an Airy disc contribution. Microroughness scatter appears to be extremely small, even at these ultraviolet wavelengths.

As noted earlier, the scattering function for the spectral bin 95 - 110 nm, is shown in Figure 3 for both the in-dispersion and cross dispersion directions, shows nearly the same angular dependence to that seen in the scattering function for the illuminated portion of the FOS grating (wavelength bins (2), (3), and (4)) except for an offset in scale of ≈ 350. Since the FOS digicon face plate consists of magnesium fluoride, with a well-known transmission cut off at 115 nm, no photons should be counted in this spectral bin. However, we see that appreciable count rates are in fact observed, and furthermore, exhibit an angular dependence similar to that seen for wavelength bins (2), (3) and (4). If this count rate were due to residual dark count, no such angular dependence would occur. We interpret this contribution as due to FOS grating scatter.

This conclusion was verified by studying the scattering characteristics of the individual FOS grating components that were measured at Johns Hopkins University, several years before integration into the FOS instrument. From a typical grating line spread function, we estimate the number of counts that might be expected in this spectral bin (1) due to grating scatter when a star is illuminating the grating over its range of sensitivity. We find that the estimated counts are consistent with the offset in count rates and their angular dependence shown in this spectral bin.

Finally, the wavelength dependence in the normalized count rates is shown for $\theta = 16''$ in Figure 5, where a higher residual count rate (~ 2 ×) is seen at the shortest wavelengths relative to the longer wavelengths. The residual spectra follow a λ^{-1} dependence. The origin of this dependence is believed to be due to the microroughness structure in the HST primary mirror[10].

In separate investigations, Hasan (1992) has concluded that the microroughness scatter from the HST does not appear to be significant at visible wavelengths. The analysis by Hasan, using WF/PC data on a bright star HD95418 (V = 2.35), with 3 different filters (F889N, F487N, and F284W) indicate that very little or no contribution occurs from microroughness scatter in the HST primary mirror. Our results also suggest that the microroughness scatter contribution is small, even at UV wavelengths, and hence indicate that the HST primary mirror surface is extremely smooth.

Acknowledgements: We greatfully acknowledge useful discussions with George Hartig, Holland Ford, Bill Fastie, and Bob Brown. This work was supported by NASA grant NAS 5-29293.

5. REFERENCES

1. Blair, W. P. et al, "Scattered Light Perpendicular to the Dispersion in the FOS", JHU CAL-FOS Report #058, Feb. 1989.

2. Brown, R. A. and Burrows, C. J., "On the Feasibility of Detecting Extra Solar Planets by Reflected Star Light using the Hubble Space Telescope", *ICARUS*, 87, 484-497, 1990.

3. Burrows, C. J., "Hubble Space Telescope Optical Telescope Assembly Handbook", Version 1.0, STScI, May, 1990.

4. Caldwell, J. "FOS/GHRS Measurements of 16 Cyg B", Dec. 1991.

5. Ebbets, D., and Heap, S. R., "Science Verification Program for the Goddard High Resolution Spectrograph of the Hubble Space Telescope:, Final Report, Ball Aerospace, Feb 24, 1992.

6. Ford, H. C., "Faint Object Spectrograph Handbook", Space Telescope Science Institute, Oct 1985.

7. Harms, R. J. et al. "Astronomical Capabilities of the Faint Object Spectrograph on Space Telescope", IAU Commission 44, The Space Telescope Observatory, Aug. 1982.

8. Harms, R. J. et al., "The Faint Object Spectrograph", SPIE, vol. 183, 74.

9. Hasan, H., "Point Spread Function Scattering Test", Instrument Science Report - OTA, STScI, Feb. 27, 1992.

10. Stover, J. C., *Optical Scattering*, McGraw Hill-New York, 1990.

11. Uomoto, A. et al. "Scattered Light Perpendicular to the Dispersion in the FOS", JHU, CAL-FOS Report #059, March 1989.

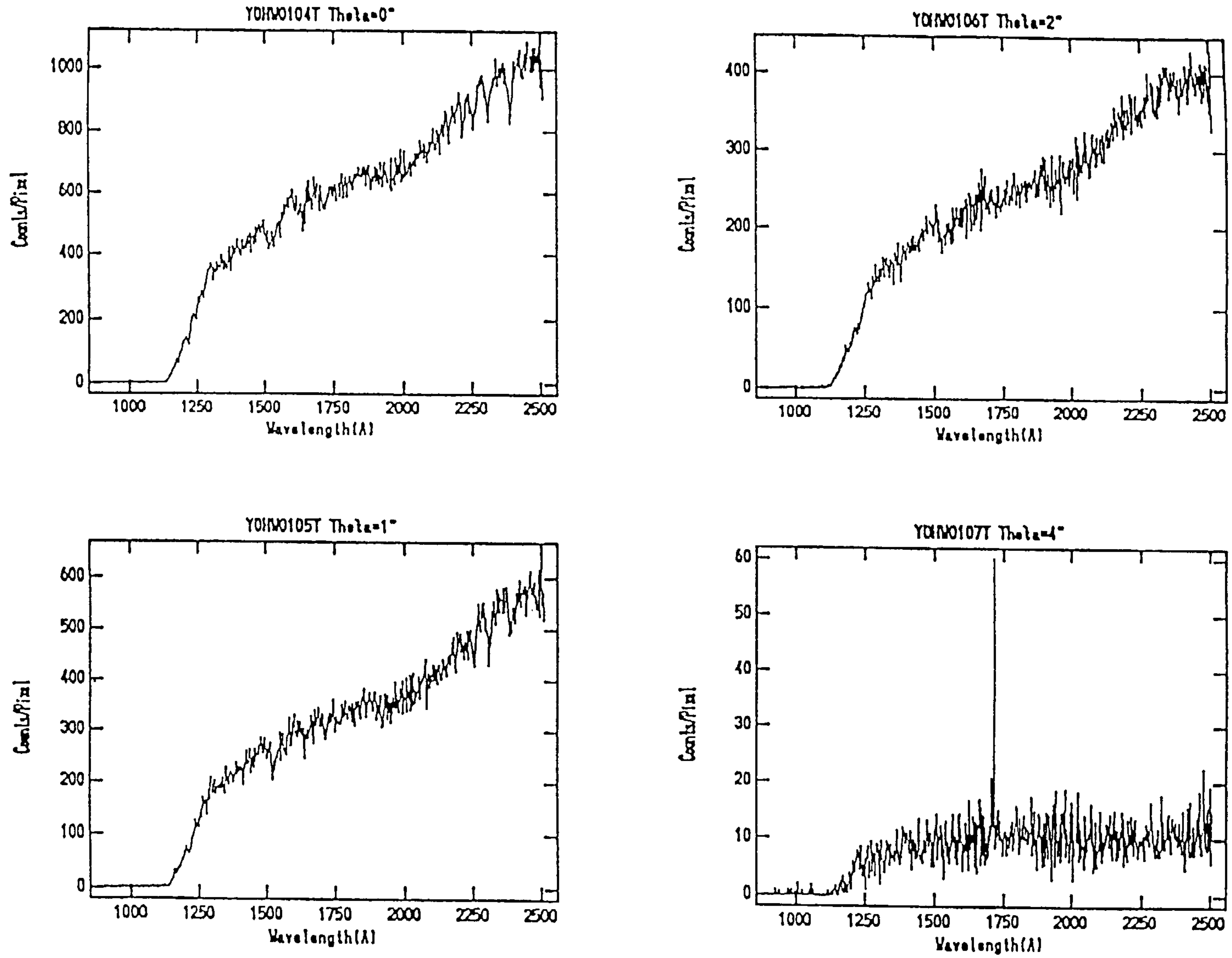

Figure 1. Spectra of standard star obtained at various offset locations (θ) in the in dispersion direction. The plots show counts versus wavelength.

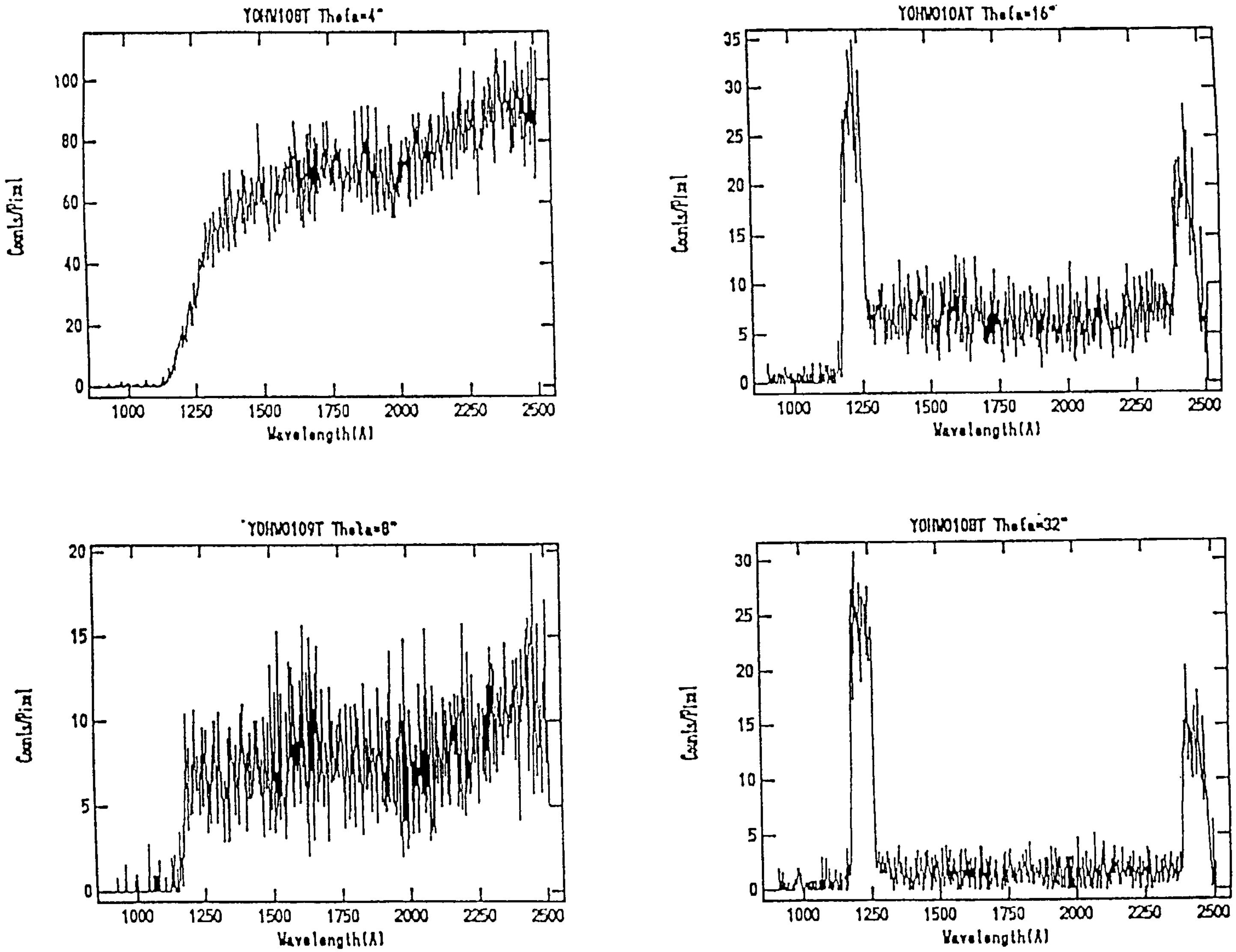

Figure 1. Spectra of standard star obtained at various offset locations (θ) in the in dispersion direction. The plots show counts versus wavelength.

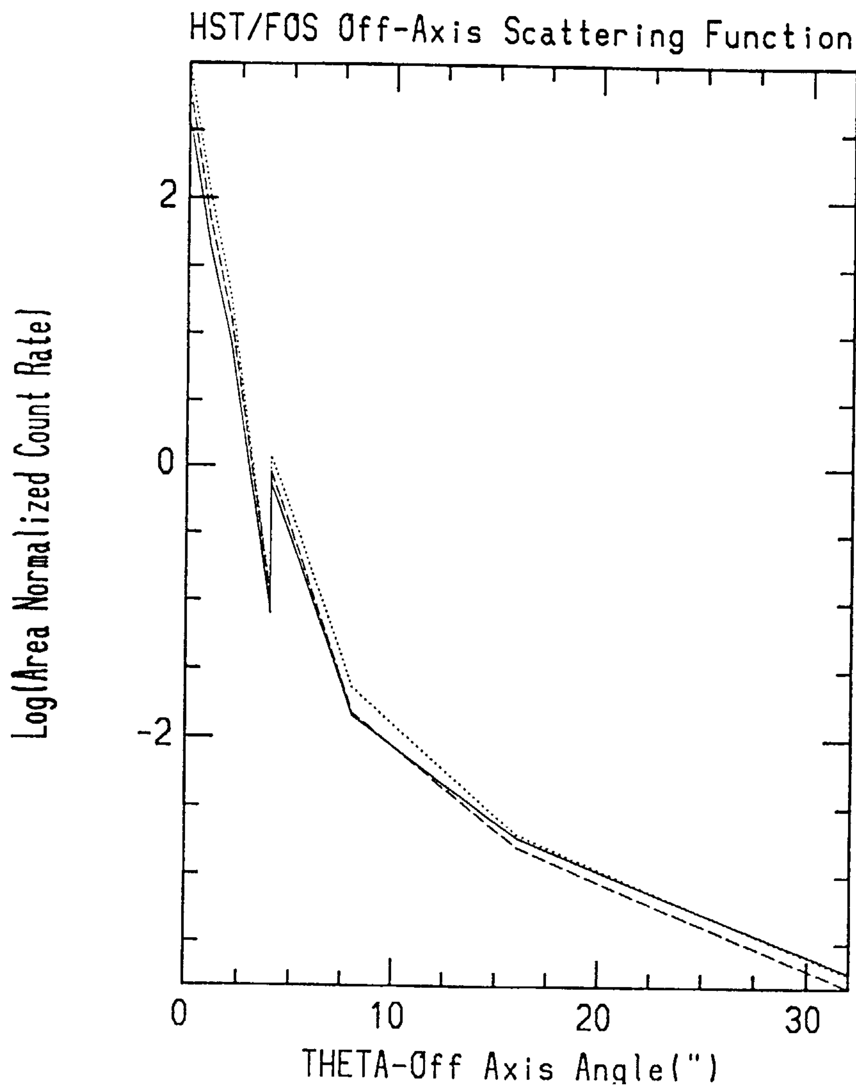

Figure 2. Normalized count rates are plotted as a function of offset positions(θ). The three curves correspond to wavelength bins 125-140nm (solid), 170-190nm (dotted), and 225-240nm (dashed). These plots represent the derived scattering function.

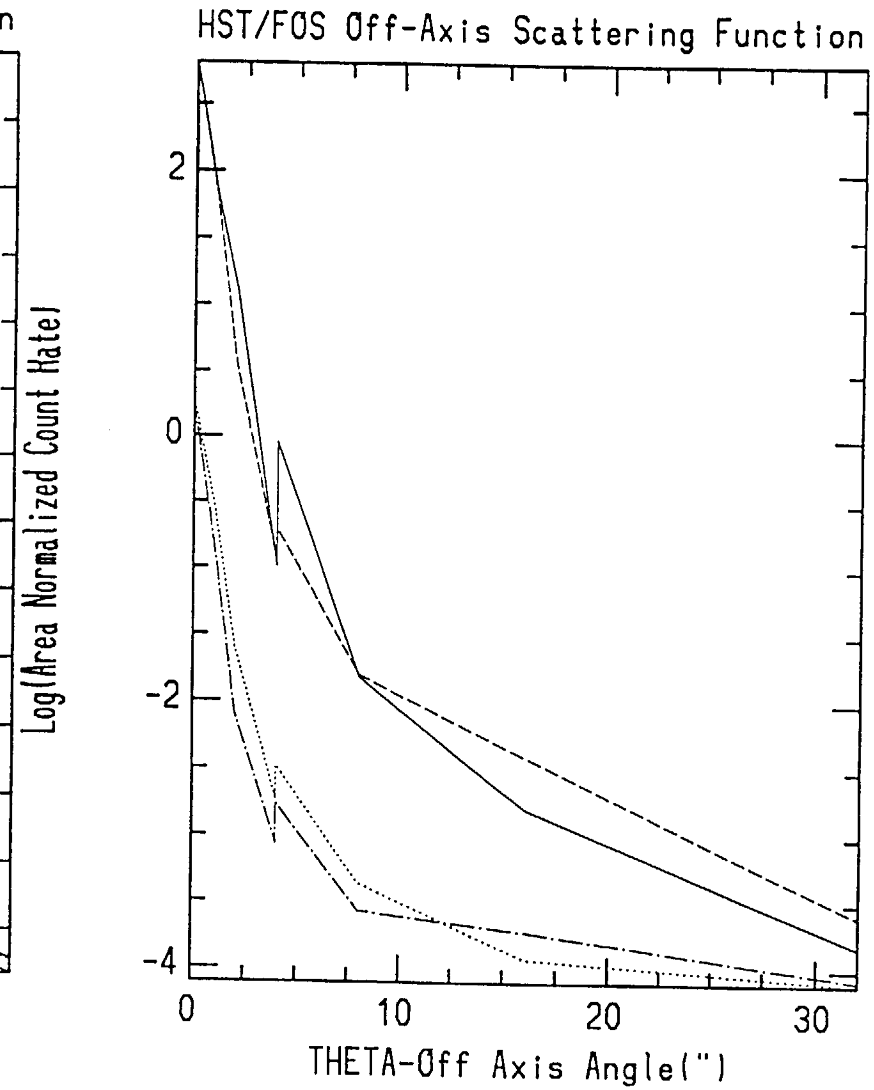

Figure 3. Normalized count rates are plotted as a function of offset positions(θ). The two sets of curves represent the wavelength bin 179-190 nm (upper set) and the bin 95-115nm (lower set) for both the in-dispersion (solid upper) and the cross dispersion directions (dotted upper).

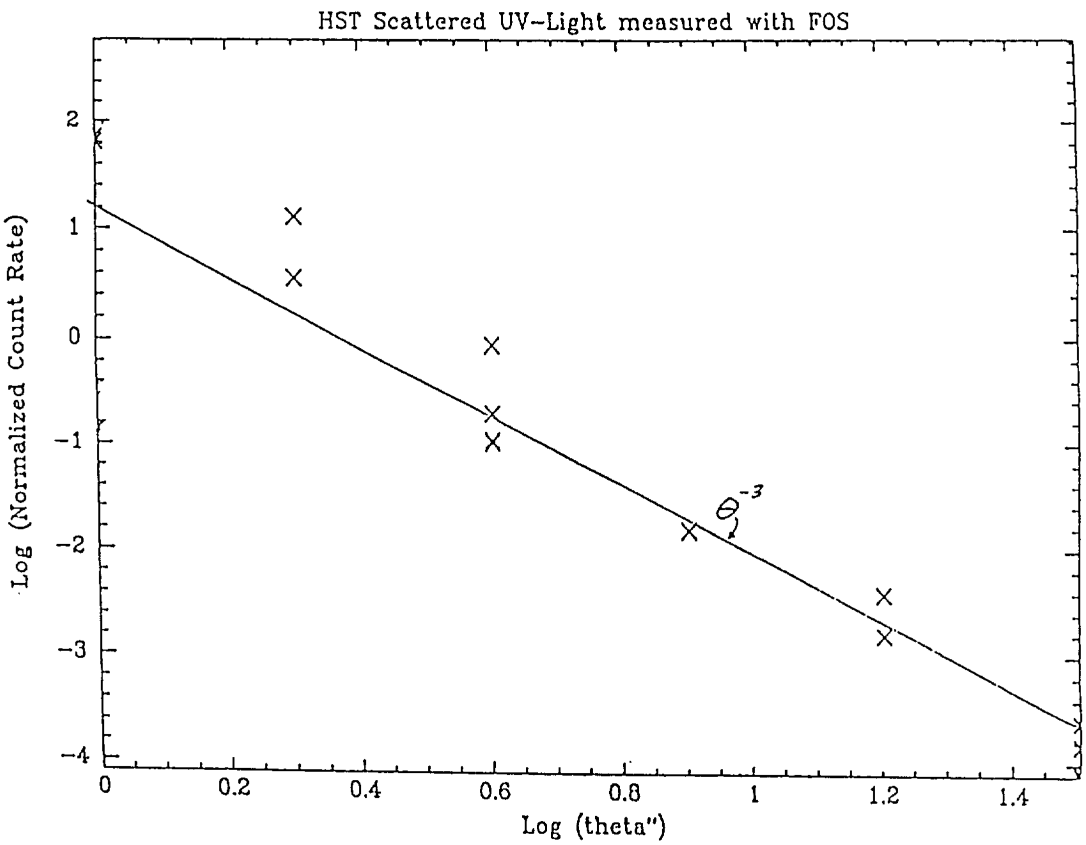

Figure 4. Power law fit to the wings of the observed scattering function. The θ^{-3} fit corresponds most closely to predictions of the Airy disk, and not to a $\theta^{-2.19}$ fit predicted by surface microroughness. This result is consistent with the λ^{-1} fit for the wavelength dependence seen in Figure 5.

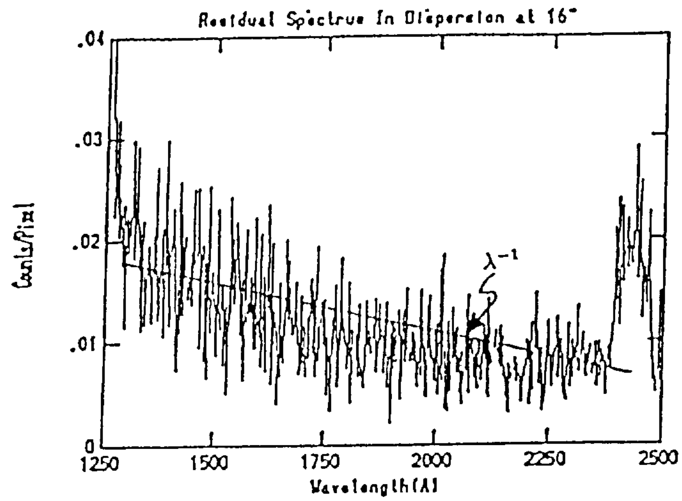

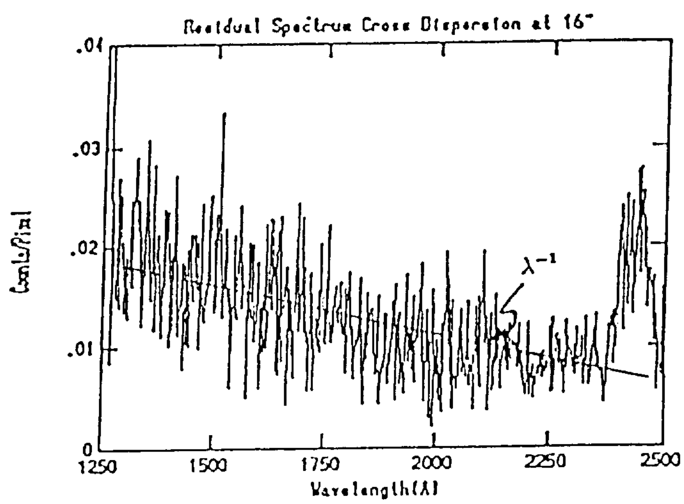

Figure 5. Residual Spectra for the offset position $\theta > 16''$, for both the in-dispersion and the cross-dispersin directions. The λ^{-1} wavelength dependence is dearly seen and consistent with very high quality smooth HST mirror surfaces.